



Comparison of contrast-enhanced ultrasound characteristics of inflammatory thyroid nodules and papillary thyroid carcinomas using a quantitative time-intensity curve: a propensity score matching analysis

Peidi Zhang^{1#}, Haijing Liu^{1#}, Xiao Yang¹, Lina Pang¹, Fen Gu¹, Jiani Yuan¹, Lei Ding¹, Jun Zhang², Wen Luo¹

¹Department of Ultrasound, Xijing Hospital, Fourth Military Medical University, Xi'an, China; ²Department of Ultrasound, New Chang'an Maternity Hospital, Xi'an, China

Contributions: (I) Conception and design: W Luo, J Zhang; (II) Administrative support: W Luo, J Zhang; (III) Provision of study materials or patients: W Luo, P Zhang, H Liu, X Yang, L Pang, F Gu, L Ding; (IV) Collection and assembly of data: P Zhang, H Liu, X Yang, L Pang, F Gu, J Yuan, L Ding; (V) Data analysis and interpretation: P Zhang, H Liu; (VI) Manuscript writing: All authors; (VII) Final approval of manuscript: All authors.

[#]These authors contributed equally to this work.

Correspondence to: Wen Luo. Department of Ultrasound, Xijing Hospital, Fourth Military Medical University, 127 Changle West Road, Xi'an 710032, China. Email: lwdd1234@fmmu.edu.cn; Jun Zhang. Department of Ultrasound, New Chang'an Maternity Hospital, 158 East Main Street, Xi'an 710032, China. Email: zj95886556@163.com.

Background: This study aims to compare the contrast-enhanced ultrasound (CEUS) characteristics of inflammatory thyroid nodules with those of papillary thyroid carcinomas using time-intensity curve (TIC) analysis.

Methods: This was a retrospective cohort study. Among the thyroid nodules in 2161 patients who underwent CEUS from July 2014 to April 2018, 44 nodules in 44 patients ultimately diagnosed as inflammatory nodules and 44 nodules in 44 patients confirmed as papillary carcinomas (enrolled from July 2016 to April 2018) were included after propensity score matching analysis (1:1). The average diameters of lesions in the inflammatory and malignant groups (n=44 each) were 0.92 ± 0.34 cm and 0.89 ± 0.42 cm, respectively. CEUS patterns were evaluated and classified into four types, namely concentric hypo-enhancement, heterogeneous hypo-enhancement, hypo-enhancement with a sharp margin, and homogeneous hyper/iso-enhancement. The measured TIC parameters included peak intensity (PI), rise time (RT), time to peak (TTP), maximum slope rate of the ascending curve (AS), and maximum slope rate of the descending curve (DS). The CEUS patterns and TIC parameters were compared between the inflammatory nodules and papillary carcinomas.

Results: The heterogeneous hypo-enhancement CEUS pattern was predominantly present in the inflammatory nodules. The concentric hypo-enhancement pattern was identified as a valuable predictive pattern for papillary carcinomas. For the TIC, inflammatory nodules had a lower PI [55.42 (45.41, 76.91) *vs.* 84.43 (74.93, 90.92)] [median (interquartile range)] and a smaller AS [22.39 (13.37, 29.93) *vs.* 29.54 (19.37, 44.77)], compared with papillary carcinomas ($P < 0.05$).

Conclusions: CEUS patterns with TIC parameters could provide effective and quantitative information for characterizing microvascular perfusion of inflammatory thyroid nodules and papillary carcinomas.

Keywords: Contrast-enhanced ultrasound (CEUS); inflammatory thyroid nodules; papillary carcinoma; time-intensity curve (TIC); propensity score matching

Submitted Dec 15, 2021. Accepted for publication Aug 09, 2022.

doi: 10.21037/qims-21-1208

View this article at: <https://dx.doi.org/10.21037/qims-21-1208>

Introduction

The prevalence of thyroid nodules has increased dramatically over the last decade. It increases with age, with a prevalence of up to 70% in the elderly, which was believed to be partly due to wider application of diagnostic imaging techniques (1). Fortunately, about 90% of detected thyroid nodules are benign, and they can be appropriately managed by follow-up evaluation without invasive procedures (2). Although fine-needle aspiration (FNA) biopsy has been used for definitive diagnosis, it cannot be ignored that a few FNA biopsies result in undetermined diagnoses or are potentially unnecessary (3,4). Therefore, accurately identifying the actual small number of malignant nodules by using a noninvasive method is crucial to avoid overdiagnosis and overtreatment of benign nodules (2,5).

High resolution gray-scale ultrasound (US) has been used in the past decade to detect thyroid nodules, with a reported accuracy of 79.6–86.08% (6,7). Based on gray-scale US features, the Thyroid Imaging Reporting and Data Systems (TIRADS) have been established worldwide to categorize risk stratification of thyroid nodules. In the recently published American College of Radiology (ACR) TIRADS (8), the presence of various sonographic features, including solid nodules, hypo-echogenicity, irregular margin, taller-than-wide shape, and microcalcifications, were considered for evaluation of suspicious malignant thyroid nodules. However, in clinical practice, these features have also been detected in some benign nodules, especially inflammatory thyroid nodules (i.e., subacute granulomatous thyroiditis-related nodules) with a diffuse change in the thyroid gland (i.e., Hashimoto's thyroiditis) (9,10). It has been noted that when thyroiditis occurs, the echogenicity of the thyroid gland becomes uneven on US images and some inflammatory nodules appear hypo-echogenic, with poorly defined margins and even dystrophic microcalcifications (11,12). After FNA biopsy for thyroid nodules associated with Hashimoto's thyroiditis, Hu *et al.* (13) reported that the overall nondiagnostic and indeterminate cytology rates were 11.9% and 25%, respectively. The areas of necrosis and inflammatory cells within nodules may interfere with the FNA results, which usually leads to the need for more than one biopsy. Further, misdiagnosis of inflammatory nodules may result in unnecessary thyroid lobectomy (10,12).

On contrast-enhanced ultrasound (CEUS) images, after injection of inert gas-filled phospholipid-based microbubbles, the microbubbles within nodules presenting a pure intravascular distribution were clearly visualized (7,14). Previous studies investigating the accuracy of CEUS in the

diagnosis of benign and malignant nodules (15–17) reported a sensitivity ranging from 85% to 88%, and a specificity ranging from 88% to 90% (18). Unfortunately, the application of CEUS in the differential diagnosis between inflammatory nodules and malignant nodules has rarely been explored. In some previous studies including a small number of inflammatory nodules, it appeared to be difficult to distinguish the hypo-enhancement CEUS pattern from that of malignant nodules (17,19). Therefore, further research is needed to develop new CEUS-based methods to differentiate inflammatory nodules from malignant nodules.

The time-intensity curve (TIC) analysis was a method that quantitatively reflected the characteristics of the entire dynamic process of tissue perfusion after microbubble contrast agent injection (15,20), with a sensitivity of 76.9%, a specificity of 84.8%, and an accuracy of 82.6% for differentiating thyroid nodules (21). Our previous study revealed that compared with benign thyroid nodules (most of which were nodular goiter cases), malignant nodules showed lower relative peak intensity (PI) values, later relative rise time (RT) values and later relative time to peak (TTP) values, and gentler relative values of the maximum slope coefficient of wash in (15). However, whether TIC analysis can provide useful information to distinguish inflammatory nodules from malignant nodules needs to be studied further.

In this cohort study, we retrospectively compared the CEUS perfusion patterns and quantitative TIC parameters between inflammatory thyroid nodules and papillary carcinomas, in order to identify the distinguishing features. We present the following article in accordance with the STROBE reporting checklist (available at <https://qims.amegroups.com/article/view/10.21037/qims-21-1208/rc>).

Methods

Patients

This was a retrospective cohort study. The study was conducted in accordance with the Declaration of Helsinki (as revised in 2013). Approval from the Institutional Review Board at Xijing Hospital was obtained before initiation of this retrospective study, and the requirement of obtaining written informed consent was waived due to the retrospective non-interventional nature of the study. From July 2014 to April 2018, 2,161 patients with thyroid nodules underwent CEUS in Xijing Hospital (Fourth Military Medical University Xi'an, China). Among them, 44 nodules in 44 patients were considered as inflammatory nodules

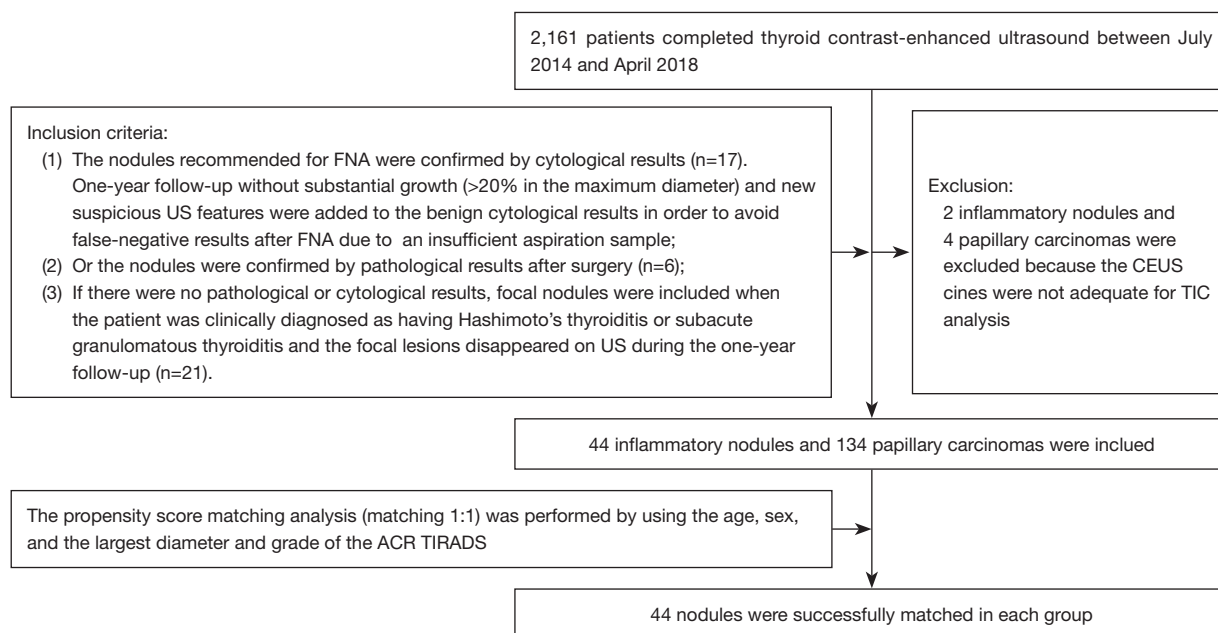


Figure 1 Consort diagram for patient selection and inclusion in the study. FNA, fine-needle aspiration; US, ultrasound; CEUS, contrast-enhanced ultrasound; TIC, time-intensity curve; ACR, American College of Radiology; TIRADS, Thyroid Imaging Reporting and Data Systems.

based on the following inclusion criteria: (I) the nodules recommended for FNA were confirmed by cytological results ($n=17$). One-year follow-up without substantial growth ($>20\%$ in the maximum diameter) and new suspicious US features were added to the benign cytological results in order to avoid false-negative results after FNA due to an insufficient aspiration sample. Ten of 17 patients with atypical clinical symptoms received FNA, and the nodules were confirmed as subacute granulomatous thyroiditis; (II) or the nodules were confirmed by pathological results after surgery ($n=6$). Before 2015, FNA was not available in our institution, and 5 patients who had nodules with TIRADS 4 or 5 underwent surgery directly and were confirmed as inflammatory nodules. After 2015, one patient with the TIRADS 5 nodule and unconfirmed cytological results received subtotal thyroidectomy due to her strong demand; (III) if there were no pathological or cytological results, focal nodules were included when the patient was clinically diagnosed as having Hashimoto's thyroiditis or subacute granulomatous thyroiditis and the focal lesions disappeared on US during the one-year follow-up ($n=21$, 11 cases of nodules in subacute granulomatous thyroiditis and 10 cases of nodules in Hashimoto's thyroiditis).

In addition, 134 nodules confirmed as papillary

carcinomas with pathological results were collected as a cohort of malignant nodules (from July 2016 to April 2018). Among them, 44 malignant nodules were finally included after the propensity score matching analysis (matching 1: 1) with 44 inflammatory nodules. The age, sex, largest diameter and grade, of the ACR TIRADS were considered in the propensity score matching analysis. The flow chart of patient enrollment is shown in *Figure 1*. Two inflammatory nodules and 4 papillary carcinomas were excluded because the CEUS cine clips were not adequate for TIC analysis. In this study, the nodule was defined as a lesion with a distinguishable margin and different echo from the surrounding tissue on gray-scale US.

CEUS examination

All US examinations were performed using a Mylab90 US imaging system (Esaote, Florence, Italy) with a LA523 linear-array probe (4–13 MHz, transmitting frequency 10 MHz) for the conventional US, and a LA522 linear-array probe (5–13 MHz, transmitting frequency 5 MHz) for CEUS. Patients were placed in the supine position, with the anterior region of the cervix fully exposed, with a light and slow breathing rhythm without swallowing. At

first, the lesion was identified by conventional US. Then, contrast-enhanced examination was performed using the Contrast Tuned Imaging (CnTI) technology, which limited the mechanical index for contrast mode and it was set at 0.03. The CnTI technology is a non-linear imaging modality optimized for harmonic signal display. When used at low acoustic pressures (set at 45 KPa), it leverages on a property of specific contrast agents, which reflects harmonics at lower pressures than tissues. Thus, this technology allows differentiation of the contrast agent from the tissue in real time. The frame rate was 8 Hz, while the output power was 3%. The dynamic compression was 2 and the edge enhancement was 3. The general gain for contrast mode was set at 50%, and time gain compensation remained in the midline. The focus position was set at the bottom of the screen. A sulfur hexafluoride (SonoVue, Bracco, Milan, Italy) suspension was quickly administered into an antebachial vein in a bolus of 1.2 mL, followed by a 10 mL 0.9% saline flush. The nodules and surrounding thyroid tissue were continuously monitored in a longitudinal section during CEUS for more than 2 min. The dynamic perfusion process of lesions and the acquired images were stored in the US equipment. For patients with multiple nodules, the most concerned or suspicious nodules were selected as the targets. The examinations were performed by two sonographers (WL and XY) with 7 and 5 years of experience in CEUS for thyroid examination.

Image analysis

The imaging data were independently analyzed by two radiologists with at least 2 years of experience in CEUS (LNP and PDZ), and they were blinded to the clinical data, as well as to the other imaging and pathology results. Enhancements on CEUS images were identified as one of the following four patterns: Concentric hypo-enhancement, which appeared as hypo-enhancement with microbubbles expanding from marginal areas of the nodule to the center (Figure 2A-2C); heterogeneous hypo-enhancement, which appeared as intra-nodular heterogeneous and hypo-echoic echogenicity, compared with the surrounding thyroid parenchyma (Figure 3A, 3B); hypo-enhancement with a sharp margin appeared as few dotted contrast enhancements within the nodule, with a clear and sharp boundary between the nodule and the surrounding areas (Figure 4A, 4B); and homogeneous hyper-enhancement/iso-enhancement was identified as intra-nodular hyper- or iso-echogenicity relative to the thyroid parenchyma, with a faint margin

(Figure 5A, 5B).

The quantitative perfusion TIC parameters were acquired by using the SonoLiver[®] v.1.0 software (TomTec GmbH, Munich, Germany), which was designed for evaluation of tissue perfusion obtained by CEUS in post-processing analysis (22). An objective quantification of the perfusion parameters with linearization was provided. Avoiding necrosis, the region of interest (ROI) for analysis on CEUS clips was selected, including the peripheral area and center area with area no less than 30% of the whole lesion. Then, the reference ROI was selected in the surrounding thyroid parenchyma near the same depth as that of the nodules, avoiding any large vessels and macro-calcifications. Only when the quality of curve fitting, which reflected matching between the initial data and the generated curve, was more than 75%, the analysis was considered valid. The echo-power signal resulted from the linearization process, and it was approximately proportional to the local US contrast agent concentration. Compared with the PI of the reference ROI that was defined as 100%, the intensity of the ROI for analysis was expressed in percentage in the Y-axis (Figure 6). Modeling consisted of fitting echo-power signals with a perfusion model function representing bolus kinetics. This model function allowed estimation of a set of perfusion parameters for quantification purposes and was defined as follows:

$$f(t) = AUC \frac{1}{st\sqrt{2\pi}} e^{-\frac{(\ln(t)-m)^2}{(2s^2)}} + O \quad [1]$$

where

$$m = \ln(mTT) - \frac{s^2}{2} \quad [2]$$

$f(t)$: best -fit function of echo-power; t : time variable; AUC : area under the curve to infinite time; mTT : mean transit time corresponding to the center of gravity of $f(t)$; s : standard deviation of the normally distributed natural logarithm of t ; O : offset amplitude.

Automatic motion compensation was used for correction of the respiratory motion. When signal from the surrounding normal parenchyma touched the ROI for analysis, the frames were deleted by the TomTech software. The perfusion parameters extracted from TICs included the following: (I) PI (the percentage ratio of the intensity of ROIs at the highest point on the TIC); (II) RT (the time from where the tangent of the ascending curve at one-half peak intersects the X-axis to PI); (III) TTP (the time from start to the PI); (IV) the maximum slope rate of the

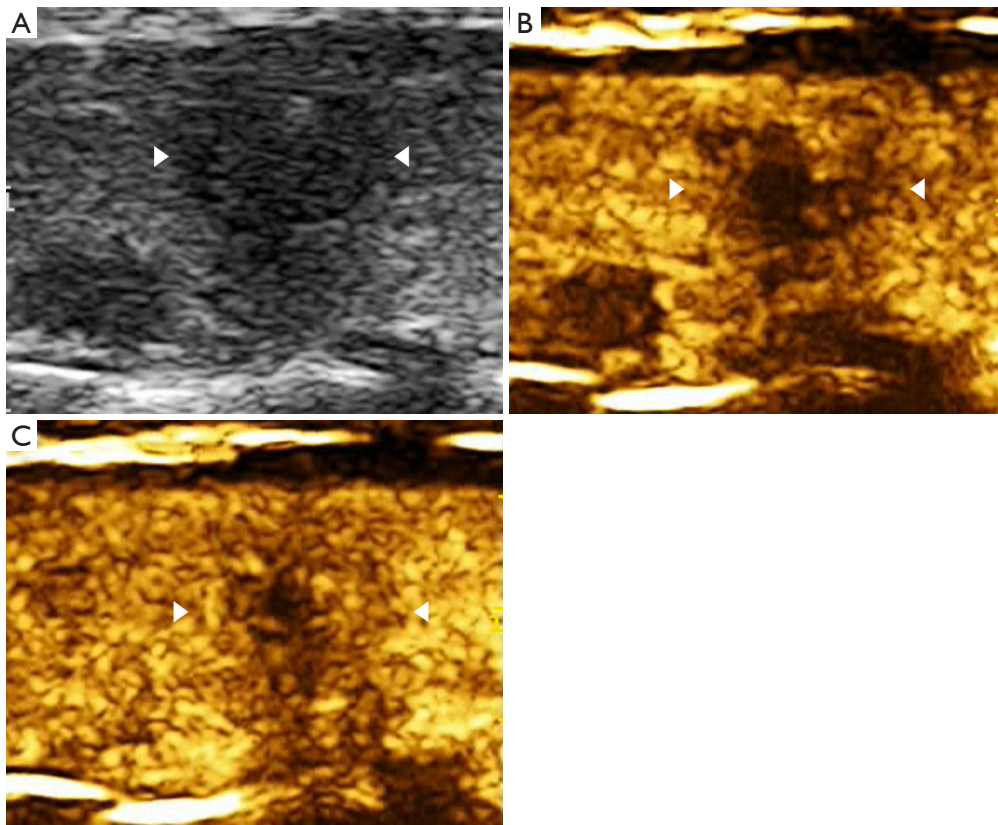


Figure 2 A thyroid papillary carcinoma (1.1 cm × 1.0 cm) in the left thyroid lobe of a 56-year-old woman was found to have concentric hypo-enhancement. (A) Conventional US showed a solid hypo-echoic nodule; (B) fourteen seconds after injection of microbubbles CEUS indicated hypo-enhancement; (C) in 20 s, the area of hypo-enhancement within the nodule shrank. Arrowheads indicate nodule margins. US, ultrasound; CEUS, contrast-enhanced ultrasound.

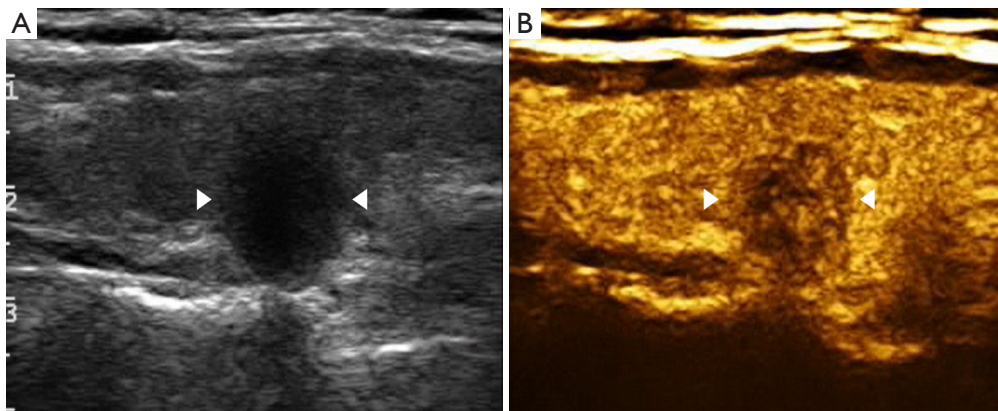


Figure 3 A thyroid nodule with pathological diagnosis of Hashimoto's thyroiditis (1.2 cm × 1.2 cm) in the right thyroid lobe of a 39-year-old woman. (A) Gray-scale US showed a hypo-echoic nodule; (B) on CEUS the nodule appeared as heterogeneous hypo-enhancement. Arrowheads indicate nodule margins. US, ultrasound; CEUS, contrast-enhanced ultrasound.

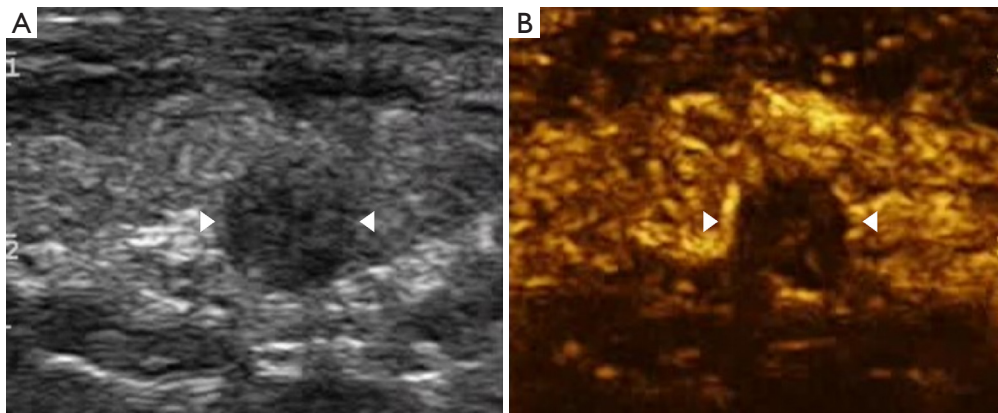


Figure 4 A 61-year-old man with a 0.6 cm × 0.7 cm solid thyroid nodule in the right lobe of his thyroid was confirmed as subacute granulomatous thyroiditis via postoperative pathological results. (A) Gray-scale US showed a hypo-echoic nodule; (B) on CEUS the nodule showed hypo-enhancement with sharp margin. Arrowheads indicate nodule margins. US, ultrasound; CEUS, contrast-enhanced ultrasound.

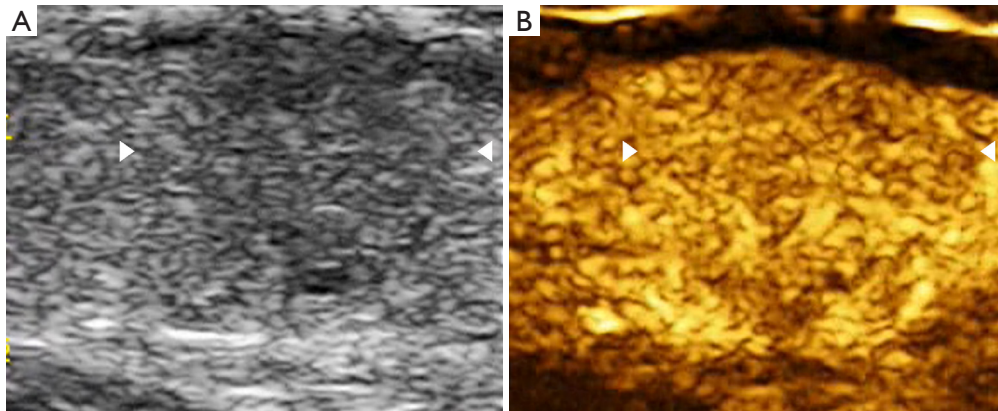


Figure 5 A 46-year-old woman with a 1.2 cm × 1.1 cm solid thyroid nodule in the right lobe of her thyroid was found was confirmed as papillary carcinoma via postoperative pathological results. (A) Conventional US showed a solid hypo-echoic nodule; (B) CEUS indicated homogeneous iso-enhancement without clear margin from the surrounding areas. Arrowheads indicate nodule margins. US, ultrasound; CEUS, contrast-enhanced ultrasound.

ascending curve (AS, the maximum of the second derivative of the ascending curve); (V) the maximum slope rate of the descending curve (DS, the minimum of the second derivative of the ascending curve). Two radiologists (LNP and PDZ), who were trained to manually select the ROIs before analysis, independently measured all parameters three times, and the average value was calculated.

Statistical analysis

The SPSS v.20.0 software (IBM Corporation, Armonk, NY, USA) was used for statistical analysis of the data.

Quantitative data of the study population were expressed as the mean ± standard deviation. Due to their non-normal distribution, TIC parameters of the nodules were presented as the number and the median with inter-quartile range for quantitative variables. Nonparametric Mann-Whitney test was used to compare the differences in sonographic features between inflammatory nodules and papillary carcinomas. The inter- and intraobserver agreements were assessed using the Kappa test. The Kappa value indicated slight consistency between 0–0.2, fair consistency between 0.2–0.4, moderate consistency between 0.4–0.6, substantial consistency between 0.6–0.8, and almost perfect consistency

between 0.8–1. All differences with a $P < 0.05$ were considered statistically significant.

Results

Study population

After propensity score matching analysis, 44 inflammatory nodules from 44 patients and 44 papillary carcinomas from 44 patients were selected for the study (Table 1). Among

inflammatory nodules, eight nodules in Hashimoto's thyroiditis and 15 nodules in subacute granulomatous thyroiditis were confirmed by postoperative pathological results or cytological results with 1-year follow-up. The other 21 inflammatory nodules were finally diagnosed with the evidence of follow-up (10 nodules in Hashimoto's thyroiditis and 11 nodules in subacute granulomatous thyroiditis). There was no difference in patient age, nodule size, and ACR TIRADS between patients with inflammatory nodules and papillary carcinomas ($P > 0.05$).

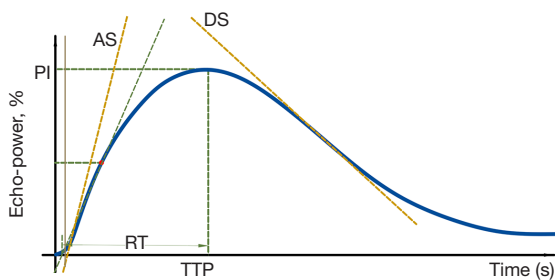


Figure 6 The curve drawing with perfusion parameters obtained from the quantitative analysis of the CEUS examination. CEUS, contrast-enhanced ultrasound; PI, peak intensity; RT, rise time; TTP, time to peak; AS, the maximum slope rate of ascending curve; DS, the maximum slope rate of descending curve.

CEUS patterns

Two radiologists evaluated the characteristics of CEUS perfusion patterns, as showing an almost perfect consistency ($\text{Kappa} = 0.884$, $P < 0.001$). There was an also almost perfect intraobserver consistency ($\text{Kappa} = 0.945$, $P < 0.001$) in the evaluation of characteristics of CEUS perfusion patterns. Significant differences were detected between the CEUS patterns of inflammatory thyroid nodules and papillary carcinomas ($P < 0.001$) (Table 2), especially in the concentric hypo-enhancement and heterogeneous hypo-enhancement patterns ($P < 0.05$). The heterogeneous hypo-enhancement pattern was demonstrated as the dominant type of pattern in inflammatory nodules (22/44), with sensitivity and specificity

Table 1 Baseline characteristics of the patients (patients $n = 88$, nodules $n = 88$)

| Category | Inflammatory | Papillary carcinoma |
|--|---------------------------|---------------------------|
| Male/female | 11/33 | 11/33 |
| Age (years), mean \pm standard deviation [range] | 48.64 \pm 8.89 [33–63] | 49.93 \pm 10.98 [28–67] |
| Nodules, number | 44 | 44 |
| The largest diameter (cm), mean \pm standard deviation (range) | 0.92 \pm 0.34 (0.4–1.8) | 0.89 \pm 0.42 (0.4–2.5) |
| Ultrasound characteristics | | |
| Solid | 44 | 44 |
| Hypoechoic/isoechoic | 42/2 | 44/0 |
| Taller-than-wide/wide-than-taller | 4/40 | 8/36 |
| Irregular/regular margin | 39/5 | 43/1 |
| Calcification with large comet tail | 1 | 1 |
| Macrocalcifications | 3 | 7 |
| ACR TIRADS | | |
| TIRADS 4 | 40 | 36 |
| TIRADS 5 | 4 | 8 |

ACR, American College of Radiology; TIRADS, Thyroid Imaging Reporting and Data Systems.

Table 2 CEUS enhancement information on thyroid nodules

| CEUS enhancement patterns | Number of nodules | Pathological results/number | | P value |
|------------------------------------|-------------------|-----------------------------|---------------------|---------|
| | | Inflammatory nodule | Papillary carcinoma | |
| Concentric hypo-enhancement | 25 | 4 | 21 | <0.001* |
| Heterogeneous hypo-enhancement | 32 | 22 | 10 | 0.010* |
| Hypo-enhancement with sharp margin | 2 | 2 | 0 | 0.155 |
| Homogeneous hyper/iso-enhancement | 29 | 16 | 13 | 0.499 |

*P<0.05 were considered as significant difference. CEUS, contrast-enhanced ultrasound.

Table 3 Comparison of quantitative TIC parameters between thyroid inflammatory nodules and papillary carcinoma

| Parameters | Inflammatory nodules | Papillary carcinoma | P value |
|------------|----------------------|----------------------|---------|
| PI | 55.42 (45.41, 76.91) | 84.43 (74.93, 90.92) | <0.001* |
| RT (s) | 4.76 (4.01, 7.05) | 6.07 (3.88, 8.20) | 0.307 |
| TTP (s) | 6.24 (4.63, 8.12) | 6.57 (4.34, 9.81) | 0.515 |
| AS | 22.39 (13.37, 29.93) | 29.54 (19.37, 44.77) | 0.013* |
| DS | -3.53 (-6.65, -2.00) | -2.98 (-7.65, -2.15) | 0.773 |

The data was presented as median (interquartile range). *P<0.05 were considered as significant difference. TIC, time-intensity curve; PI, peak intensity; RT, rise time; TTP, time to peak; AS, the maximum slope rate of ascending curve; DS, the maximum slope rate of descending curve.

values of 50% and 77%, respectively. The concentric hypo-enhancement pattern was identified as the dominant type of pattern in papillary carcinomas (21/44), with sensitivity and specificity values of 47.7% and 90.9%, respectively. Hypo-enhancement with a sharp margin was detected in 2 inflammatory nodules but not in papillary carcinomas. The homogeneous hyper-enhancement/iso-enhancement pattern failed to achieve statistical significance between inflammatory nodules and papillary carcinomas (P>0.05).

Quantitative TIC parameters

Compared to the TIC analysis parameters of all papillary carcinomas (Table 3), those of inflammatory nodules had a lower PI and smaller AS (P<0.05) (Figure 7A-7D, Figure 8A-8D). Inflammatory nodules appearing as heterogeneous hypo-enhancement (n=22) also had a lower PI and smaller AS (P<0.05), when compared to papillary carcinomas presenting as heterogeneous hypo-enhancement (n=10). There was no statistically significant difference in the RT, TTP, and DS (P>0.05). When presenting as the homogeneous hyper-enhancement/iso-enhancement pattern, the inflammatory nodules (n=16) also had a lower

PI when compared to the papillary carcinomas (n=13) (P<0.05) (Table 4).

Discussion

In this study, in order to further investigate the characteristics of inflammatory nodules and malignant nodules, CEUS with TIC analysis was performed in 88 thyroid nodules by using propensity score matching analysis. It was detected that the heterogeneous hypo-enhancement pattern was predominant in inflammatory nodules, whereas the concentric hypo-enhancement pattern was predominant in papillary carcinomas. Compared to the TIC parameters of papillary carcinomas, the PI and AS of inflammatory nodules were lower, which may be useful for differentiation and complementing the results of CEUS.

In clinical practice, information based on the interpretation of gray-scale US images may not be adequate for differentiating thyroid nodules, especially when diffusion changes have occurred in the thyroid gland. In this study, more than 50% of the inflammatory nodules were detected with diffuse thyroid changes, which made it difficult to perform an evaluation by only relying

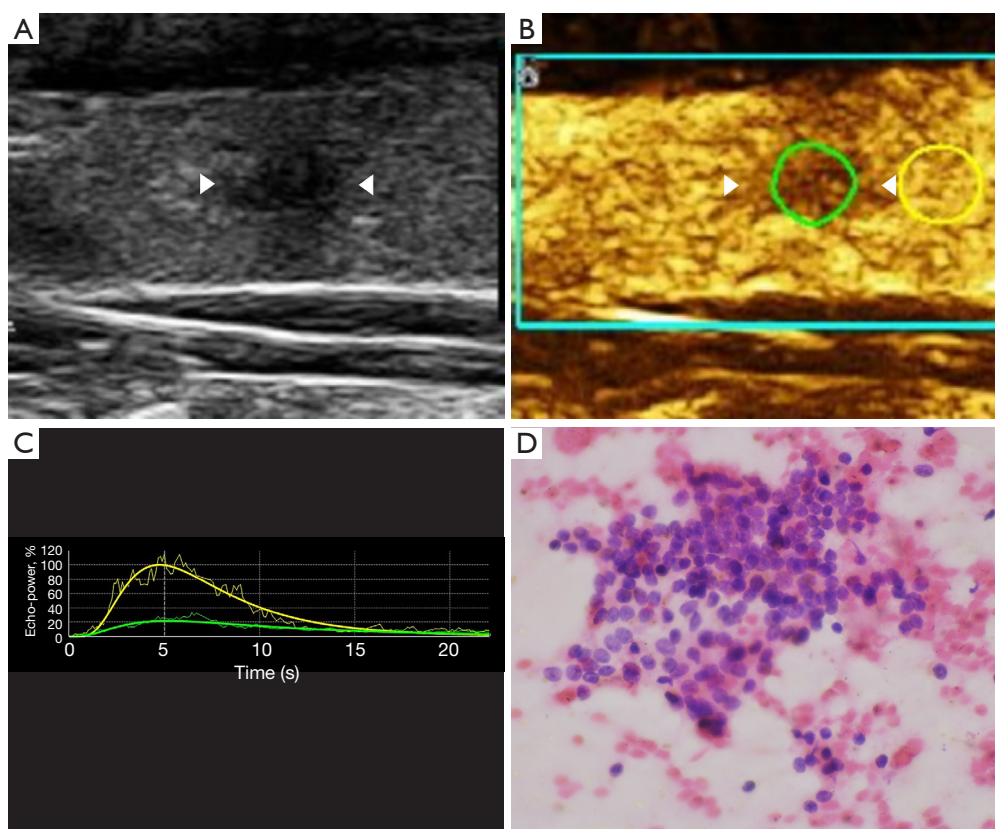


Figure 7 A 53-year-old woman with a 0.9 cm × 0.7 cm solid thyroid nodule in the left lobe of her thyroid was confirmed as Hashimoto's thyroiditis via cytological results and the focal lesion disappeared during one-year follow-up. ROI was selected in the reference area (yellow lines) and analysis area (green lines). Arrowheads indicate nodule margins. (A) Conventional US image; (B) CEUS image; (C) dynamic perfusion curves; (D) cytopathologic image (hematoxylin-eosin staining, ×40). ROI, region of interest; US, ultrasound; CEUS, contrast-enhanced ultrasound.

on gray-scale US. To provide more useful information for diagnosis, CEUS that presents microvascularity has attracted much attention recently. On CEUS, patterns of heterogeneous hypo-enhancement and hypo-enhancement with a sharp margin were presented in 54.5% (24/44) of the inflammatory nodules, which reflected hypo-perfusion and lower vascularity of most of the inflammatory nodules. Histologically, Hashimoto's thyroiditis and subacute granulomatous thyroiditis were characterized by interstitial infiltration of inflammatory cells, including multinucleated giant cells, lymphocytes, and neutrophils, and a variable degree of fibrosis in the interstitium (23,24), which may be the cause of heterogeneous echogenicity on US imaging and low vascularity on CEUS. On the other hand, 36.3% (16/44) of the inflammatory nodules presented homogeneous hyper-enhancement/iso-enhancement. Among them, 12 nodules were finally related to Hashimoto's thyroiditis and

4 were related to subacute granulomatous thyroiditis. In these nodules, local fibrosis may not have yet occurred and lymphocytic infiltration was minimal in focal areas, which may have resulted in vascular proliferation (11).

In the current study, the hypo-enhancement with a sharp margin pattern was observed in two inflammatory nodules, and one of them was a Hashimoto's thyroiditis-related nodule and the other was a subacute granulomatous thyroiditis-related nodule. This pattern was also reported in our previous study and not presented in malignant ones (17). Tissue necrosis and exudation due to inflammation were considered to be related with hypo-enhancement and clearly demarcated the nodule from the normal tissue. In a previous study, we also observed the hypo-enhancement with a sharp margin pattern in nodular goiter with high specificity (17). Therefore, the hypo-enhancement with a sharp margin pattern could be regarded as a typical pattern in benign

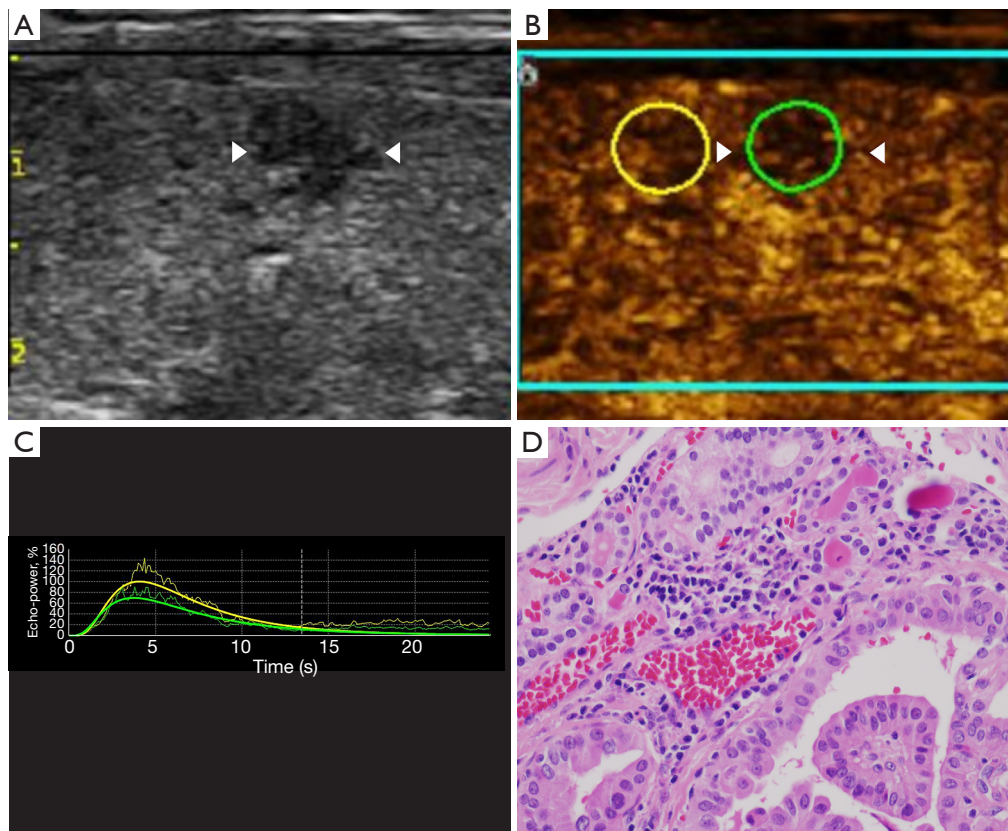


Figure 8 A 28-year-old man with a 0.7 cm × 0.6 cm solid thyroid nodule in the right lobe of his thyroid was confirmed as papillary carcinoma via postoperative pathological results. ROI was selected in the reference area (yellow lines) and analysis area (green lines). Arrowheads indicate nodule margins. (A) Conventional US image; (B) CEUS image; (C) dynamic perfusion curves; (D) histopathologic image (hematoxylin-eosin staining, ×40). ROI, region of interest; US, ultrasound; CEUS, contrast-enhanced ultrasound.

Table 4 Comparison of quantitative TIC parameters of heterogeneous hypo-enhancement and homogeneous hyper/iso-enhancement between thyroid inflammatory nodules and papillary carcinoma

| Parameters | Heterogeneous hypo-enhancement | | | Homogeneous hyper/iso-enhancement | | |
|------------|--------------------------------|----------------------|---------|-----------------------------------|-----------------------|---------|
| | Inflammatory nodules | Papillary carcinoma | P value | Inflammatory nodules | Papillary carcinoma | P value |
| PI | 51.15 (38.82, 58.78) | 81.3 (73.15, 92.46) | <0.001* | 73.18 (63.74, 87.34) | 90.71 (84.50, 105.87) | 0.003* |
| RT (s) | 5.03 (4.00, 8.11) | 4.36 (3.25, 7.19) | 0.962 | 4.54 (3.98, 6.20) | 5.10 (3.72, 11.79) | 0.129 |
| TTP (s) | 6.43 (4.64, 9.35) | 4.97 (3.67, 8.19) | 0.854 | 5.58 (4.54, 6.90) | 6.22 (4.18, 12.69) | 0.100 |
| AS | 17.95 (10.27, 23.21) | 32.09 (15.58, 51.40) | 0.016* | 29.83 (23.11, 38.23) | 35.75 (12.76, 51.00) | 0.501 |
| DS | -2.92 (-4.76, -1.47) | -3.81 (-7.89, -2.14) | 0.595 | -4.97 (-8.03, -2.31) | -4.90 (-10.69, -1.93) | 0.567 |

The data was presented as median (interquartile range). *P<0.05 were considered as significant difference. TIC, time-intensity curve; PI, peak intensity; RT, rise time; TTP, time to peak; AS, the maximum slope rate of ascending curve; DS, the maximum slope rate of descending curve.

nodules. Instead, concentric hypo-enhancement was the predominant pattern in papillary carcinomas, accounting for 47.7% (21/44) of the nodules in the present study, which was consistent with the findings reported by other researchers (25). This suggests that the blood vessels in the peripheral zone of the lesion were relatively dense, but they were sparse in the center; and thus, neovascularization was non-uniformly distributed in the entire lesion (26).

Although CEUS patterns presented differences between inflammatory nodules and malignant nodules, it was confusing to distinguish CEUS patterns of heterogeneous hypo-enhancement or concentric hypo-enhancement for small size nodules. In the current study, TIC parameters were investigated to provide supplementary information. Previously, we detected that malignant nodules had lower relative values of PI and relative values of maximum slope coefficient of wash-in compared with benign nodules, which reflected poor vascularity in the malignant group (15). However, in this study, a lower PI ($P < 0.05$), inferior AS ($P < 0.05$), and longer RT and TTP ($P > 0.05$) demonstrated lower perfusion of microbubbles in the inflammatory groups than in the malignant groups. We also detected that even inflammatory nodules in the homogeneous hyper-enhancement/iso-enhancement pattern had a lower PI compared with malignant nodules in homogeneous enhancement. These results indicated decreased vascularity within inflammatory nodules. In this study, most of the inflammatory nodules resulted from chronic thyroiditis. It was conjectured that infiltration of massive inflammatory cells and fibrogenesis occurred in chronic inflammatory nodules compared to vessels that developed in malignant nodules (23,24). On the other hand, the structure of vessels in malignant tissue was different from that in the benign ones, which was reflected in our results suggesting that more nodules in the malignant group presented concentric hypo-enhancement than those in the inflammatory group. Therefore, TIC parameters could be helpful to quantitatively provide complementary information for the results of CEUS patterns in order to characterize microvasculature of inflammatory and malignant nodules.

In this study, the average nodule size was less than 1 cm. Nodules with a diameter of less than 1 cm may not be suitable for FNA biopsies or may be easily missed, which made it difficult to make a diagnosis decision in clinical practice. The results of this study on CEUS may provide supplementary information for image evaluation of these small nodules. In addition, all patients with subacute granulomatous thyroiditis in this study were cases of

atypical subacute granulomatous thyroiditis, without any hallmark symptom, such as fever and cervical pain. The CEUS results of this study may be helpful for diagnosis of these nodules without typical symptoms.

This study has the following limitations: First, in this retrospective study, some patients with inflammatory nodules were excluded due to lack of confirmed results or follow-up. Selective bias could not be completely ruled out in this study. Second, when the images were retrospectively collected, the inevitable noise of the TIC curve appeared in some cases due to the respiratory motion and scanning procedure, although motion correction was performed. Third, despite providing some useful information to distinguish features between the two types of nodules, there may be some subjective factors in image judgment and US performance. Fourth, a large-scale prospective diagnosis research is needed to confirm these findings and evaluate the threshold of TIC parameters in the future. Finally, limitations of propensity score matching associated with limited covariate overlap may be especially pronounced. The missing data in the malignant groups may interfere with the representativeness of samples.

Conclusions

CEUS patterns with TIC parameters could provide effective and quantitative information for characterizing microvascular perfusion of inflammatory thyroid nodules and papillary carcinomas.

Acknowledgments

Funding: This work was supported by the National Science Foundation of China (No. 81671691).

Footnote

Reporting Checklist: The authors have completed the STROBE reporting checklist. Available at <https://qims.amegroups.com/article/view/10.21037/qims-21-1208/rc>

Conflicts of Interest: All authors have completed the ICMJE uniform disclosure form (available at <https://qims.amegroups.com/article/view/10.21037/qims-21-1208/coif>). The authors have no conflicts of interest to declare.

Ethical Statement: The authors are accountable for all aspects of the work in ensuring that questions related

to the accuracy or integrity of any part of the work are appropriately investigated and resolved. The study was conducted in accordance with the Declaration of Helsinki (as revised in 2013). Approval from the Institutional Review Board at Xijing Hospital was obtained before initiation of this retrospective study, and the requirement of obtaining written informed consent was waived due to the retrospective non-interventional nature of the study.

Open Access Statement: This is an Open Access article distributed in accordance with the Creative Commons Attribution-NonCommercial-NoDerivs 4.0 International License (CC BY-NC-ND 4.0), which permits the non-commercial replication and distribution of the article with the strict proviso that no changes or edits are made and the original work is properly cited (including links to both the formal publication through the relevant DOI and the license). See: <https://creativecommons.org/licenses/by-nc-nd/4.0/>.

References

- Walsh JP. Managing thyroid disease in general practice. *Med J Aust* 2016;205:179-84.
- Durante C, Grani G, Lamartina L, Filetti S, Mandel SJ, Cooper DS. The Diagnosis and Management of Thyroid Nodules: A Review. *JAMA* 2018;319:914-24.
- Haugen BR, Alexander EK, Bible KC, Doherty GM, Mandel SJ, Nikiforov YE, Pacini F, Randolph GW, Sawka AM, Schlumberger M, Schuff KG, Sherman SI, Sosa JA, Steward DL, Tuttle RM, Wartofsky L. 2015 American Thyroid Association Management Guidelines for Adult Patients with Thyroid Nodules and Differentiated Thyroid Cancer: The American Thyroid Association Guidelines Task Force on Thyroid Nodules and Differentiated Thyroid Cancer. *Thyroid* 2016;26:1-133.
- Zhu H, Yang Y, Wu S, Chen K, Luo H, Huang J. Diagnostic performance of US-based FNAB criteria of the 2020 Chinese guideline for malignant thyroid nodules: comparison with the 2017 American College of Radiology guideline, the 2015 American Thyroid Association guideline, and the 2016 Korean Thyroid Association guideline. *Quant Imaging Med Surg* 2021;11:3604-18.
- Wang Y, Lei KR, He YP, Li XL, Ren WW, Zhao CK, Bo XW, Wang D, Sun CY, Xu HX. Malignancy risk stratification of thyroid nodules: comparisons of four ultrasound Thyroid Imaging Reporting and Data Systems in surgically resected nodules. *Sci Rep* 2017;7:11560.
- Moon HJ, Sung JM, Kim EK, Yoon JH, Youk JH, Kwak JY. Diagnostic performance of gray-scale US and elastography in solid thyroid nodules. *Radiology* 2012;262:1002-13.
- Palaniappan MK, Aiyappan SK, Ranga U. Role of Gray Scale, Color Doppler and Spectral Doppler in Differentiation Between Malignant and Benign Thyroid Nodules. *J Clin Diagn Res* 2016;10:TC01-6.
- Tessler FN, Middleton WD, Grant EG, Hoang JK, Berland LL, Teefey SA, Cronan JJ, Beland MD, Desser TS, Frates MC, Hammers LW, Hamper UM, Langer JE, Reading CC, Scoutt LM, Stavros AT. ACR Thyroid Imaging, Reporting and Data System (TI-RADS): White Paper of the ACR TI-RADS Committee. *J Am Coll Radiol* 2017;14:587-95.
- Frates MC, Marqusee E, Benson CB, Alexander EK. Subacute granulomatous (de Quervain) thyroiditis: grayscale and color Doppler sonographic characteristics. *J Ultrasound Med* 2013;32:505-11.
- Lee MY, Lam WW, Wong WY. Subacute Thyroiditis—An Often Overlooked Sonographic Diagnosis: Report of 3 Cases. *J Ultrasound Med* 2016;35:1095-100.
- Carbone A, Rotondi M, Chiovato L. Chronic Autoimmune Thyroiditis. In: Luster M, Duntas L, Wartofsky L, editors. *The Thyroid and Its Diseases*. Cham: Springer; 2019.
- Pan FS, Wang W, Wang Y, Xu M, Liang JY, Zheng YL, Xie XY, Li XX. Sonographic features of thyroid nodules that may help distinguish clinically atypical subacute thyroiditis from thyroid malignancy. *J Ultrasound Med* 2015;34:689-96.
- Hu F, Yan Z, Ma B, Jiang Y, Huang H. The impact of concurrent Hashimoto thyroiditis on thyroid nodule cytopathology assessed by ultrasound-guided fine-needle aspiration cytology. *Postgrad Med* 2020;132:506-11.
- Chen X, Hao F, Gui Y, Zhang J, Tan L, Xiao M, Zhang Q, Meng H, Li J, Jiang Y, Lv K. Enhancement patterns in the venous phase of contrast-enhanced ultrasounds: diagnostic value for patients with solid pancreatic lesions. *Quant Imaging Med Surg* 2021;11:4321-33.
- Gu F, Han L, Yang X, Liu H, Li X, Guo K, Zhao Z, Zhou X, Luo W. Value of time-intensity curve analysis of contrast-enhanced ultrasound in the differential diagnosis of thyroid nodules. *Eur J Radiol* 2018;105:182-7.
- Zhang Y, Zhou P, Tian SM, Zhao YF, Li JL, Li L. Usefulness of combined use of contrast-enhanced ultrasound and TI-RADS classification for the differentiation of benign from malignant lesions of thyroid nodules. *Eur Radiol* 2017;27:1527-36.
- Luo W, Yang X, Yuan J, Pang L, Zhang P, Ding L,

- Gu F, Liu H, Zhang Y. Evaluation of characteristics of thyroid nodules on contrast-enhanced ultrasonography: a retrospective analysis of 252 cases. *Med Ultrason* 2020;22:164-70.
18. Zhan J, Ding H. Application of contrast-enhanced ultrasound for evaluation of thyroid nodules. *Ultrasonography* 2018;37:288-97.
 19. Peng Q, Niu C, Zhang M, Peng Q, Chen S. Sonographic Characteristics of Papillary Thyroid Carcinoma with Coexistent Hashimoto's Thyroiditis: Conventional Ultrasound, Acoustic Radiation Force Impulse Imaging and Contrast-Enhanced Ultrasound. *Ultrasound Med Biol* 2019;45:471-80.
 20. Zhou X, Zhou P, Hu Z, Tian SM, Zhao Y, Liu W, Jin Q. Diagnostic Efficiency of Quantitative Contrast-Enhanced Ultrasound Indicators for Discriminating Benign From Malignant Solid Thyroid Nodules. *J Ultrasound Med* 2018;37:425-37.
 21. Diao X, Zhan J, Chen L, Chen Y, Liu Y. Quantification of solid hypo-echoic thyroid nodule enhancement with contrast-enhanced ultrasound. *Transl Cancer Res* 2017;6:1078-87.
 22. Pei XQ, Liu LZ, Liu M, Zheng W, Han F, Li AH, Cai MY. Contrast-enhanced ultrasonography of hepatocellular carcinoma: correlation between quantitative parameters and histological grading. *Br J Radiol* 2012;85:e740-7.
 23. Stathatos N. Inflammatory Diseases of the Thyroid Gland. In: *Pathobiology of Human Disease: A Dynamic Encyclopedia of Disease Mechanisms* 2014:1196-205.
 24. Prajapati S, Hernandez-Prera JC. Putting All the Pieces Together: Clinical, Macroscopic and Microscopic Characteristics of Subacute Thyroiditis. *Head Neck Pathol* 2019;13:231-4.
 25. Wu Q, Wang Y, Li Y, Hu B, He ZY. Diagnostic value of contrast-enhanced ultrasound in solid thyroid nodules with and without enhancement. *Endocrine* 2016;53:480-8.
 26. Yuan Z, Quan J, Yunxiao Z, Jian C, Zhu H. Contrast-enhanced ultrasound in the diagnosis of solitary thyroid nodules. *J Cancer Res Ther* 2015;11:41-5.

Cite this article as: Zhang P, Liu H, Yang X, Pang L, Gu F, Yuan J, Ding L, Zhang J, Luo W. Comparison of contrast-enhanced ultrasound characteristics of inflammatory thyroid nodules and papillary thyroid carcinomas using a quantitative time-intensity curve: a propensity score matching analysis. *Quant Imaging Med Surg* 2022;12(11):5209-5221. doi:10.21037/qims-21-1208